



Kinetic modeling of adsorption of vanadium and iron from acid solution through ion exchange resins

José Helber VINCO, Amilton Barbosa BOTELHO JUNIOR, Heitor Augusto DUARTE,
Denise Crocce Romano ESPINOSA, Jorge Alberto Soares TENÓRIO

Department of Chemical Engineering, Polytechnic School of the University of São Paulo (USP),
Rua do Lago, 250, 05508-080, São Paulo, SP, Brazil

Received 26 July 2021; accepted 14 March 2022

Abstract: This study assessed the adsorption process and the reaction kinetics involved in the selective recovery of vanadium from an acid solution containing iron as an impurity. Four commercial resins were studied: Lewatit® MonoPlus TP 209 XL, Lewatit® TP 207, Dowex™ M4195 (chelating resin) and Lewatit® MonoPlus S 200 H (strong cationic exchange resin). To investigate the effect of time on the adsorption process, batch experiments were carried out using the following initial conditions: pH 2.0, 298 K, and a proportion of 1 g of resin to 50 mL of solution. The variation of pH over time was analyzed. Chelating resin released less H⁺ ions as the adsorption occurred, resulting in a lower drop of pH when compared to S 200 H resin. Ion adsorption by the resins was also evaluated through FT-IR and SEM-EDS before and after the experiments. Among the evaluated kinetic models (pseudo-first order, pseudo-second order, Elovich and intraparticle diffusion models), the pseudo-second order model best fits the experimental data of the adsorption of vanadium and iron by all of the four resins. M4195 resin showed the highest recovery of vanadium and the lowest adsorption of iron. Kinetic data, which are fundamental to industrial processes applications, are provided.

Key words: vanadium recovery; adsorption; chelating resins; metal ions; cation exchange resin; batch experiments

1 Introduction

One of the main applications of vanadium is as an additive in steel alloys (e.g, ferrovanadium) which represents a consumption over 80% of the global production [1,2]. Vanadium has been standing out and getting more space for storage batteries on a large scale, especially from renewable sources, which causes the growth on its demand in the coming years [3,4]. Vanadium consumption for electrolyte production is estimated to grow by as much as 44% by the year 2027 as these batteries gain more visibility [5].

Vanadium occurs predominantly in the form of V³⁺ replacing Fe³⁺ or Al³⁺ in several minerals in ore deposits and crude oil. In addition, metallurgical

slags have become other important source for obtaining vanadium [3]. Regardless of the origin, impurities will be associated in the vanadium extraction, which reflects in a necessity for methods to purify and obtain products with high purity, especially for application in electrolytes of vanadium redox flow batteries. However, there is a lack in the literature of deep studies about the influence of impurities on the battery's performance. Therefore, these applications still require a product with purity above 99.8%, greatly increasing its cost [6].

There are several studies aimed at the purification of solutions containing vanadium and other impurities using techniques such as solvent extraction [7–12], chemical precipitation [13–15] and ion exchange resins [16–20]. A comparison

among these methods for recovering vanadium from leach liquors was also critically reviewed in the work by ZHANG et al [21].

In this context, ion exchange resins stand out, especially chelating resins, considering that the ion exchange technique applied to the recovery of strategic metals is among the fundamental technologies for the development and progress of society [22]. Ion exchange was linked to several modern technologies, being widely used in several industrial applications which include advanced separations, such as metal recovery, water treatment and removal of radioactive isotopes [23]. In addition to their extensive industrial use [24], ion exchange resins offer advantages such as low energy cost, simplicity in operation and fast kinetics, reflecting a low operating cost [25].

There are several commercial resins available designed to recover different metals [26]. Cationic, anionic and chelating resins are used in different purification processes, and chelators in chelating resins have been developed to improve the selectivity of the process. The order of selectivity of these resins depends on their functional groups [25]. An electrostatic interaction between functional group and the adsorbed metal occurs by donor atoms present in their functional groups, such as nitrogen, sulfur, oxygen and phosphorus, which have pairs of unemployed electrons and form coordinated links with adsorbed metals [27,28].

The investigation of the adsorption process by kinetic modeling is crucial, owing to ideal conditions of operation in large-scale batch, mechanism of sorption between the metal and the resin, and control of the reaction rate including mass transportation and chemical reaction processes [29,30]. FEBRIANTO et al [31] stated that, in projects of an adsorption system, the knowledge of the adsorption rate involved in the recovery of a metal by a certain resin figure among the most important steps, because, from this study, the time of residence of the adsorbate is known.

Besides, the kinetic modeling is important to evaluate the separation rate between vanadium and contaminants. Therefore, this study is devoted to investigate the adsorption and model adsorption kinetics of iron and vanadium by ion exchange resins. Three chelating resins and one strong cationic resin were tested. The kinetic investigation was performed through the evaluation of four

kinetic models (pseudo-first order, pseudo-second order, Elovich and intraparticle diffusion). FT-IR and SEM-EDS analyses were used as chemical characterization of the resins to enhance the interpretation of the process.

2 Experimental

2.1 Ion exchange resins and synthetic solution

Four ion exchange resins were used: Lewatit[®] MonoPlus TP 209 XL, Lewatit[®] TP 207, Dowex[™] M4195 and Lewatit[®] MonoPlus S 200 H. These resins are functionalized by the following functional groups: iminodiacetic acid, iminodiacetic acid, bis-picolyamine and sulfonic acid, respectively. Figure 1 depicts the structures of these groups.

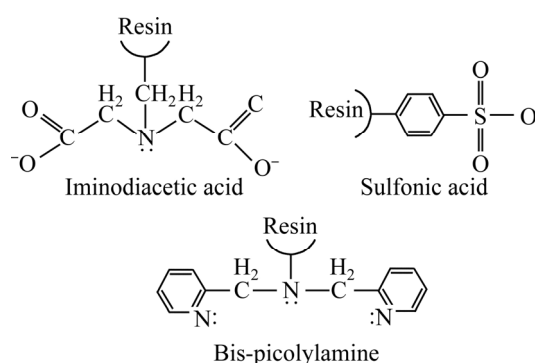


Fig. 1 Functional groups of resins: iminodiacetic acid (TP 209 XL and TP 207 resins), sulfonic acid (S 200 H resin) and bis-picolyamine (M4195 resin)

A pre-treatment step was performed previously to the experiments to eliminate any possible remnant impurity of the resins manufacture and to obtain H⁺ exchangeable ions. The pre-treatment consisted in washing the resins with hydrochloric acid solution (4 mol/L HCl) interspersed with three-fold deionized water. The washing process was conducted in Erlenmeyer flasks (250 mL) in orbital shaker (200 r/min) under a temperature of 298 K at intervals of 4 h for each wash. After the last wash with water, flasks were taken to an ultrasonic bath for 10 min. Finally, the resins were separated by filtration and dried at 333 K for 24 h.

The synthetic solution was prepared by the dissolution of 10 g of commercial vanadium pentoxide (V₂O₅, 99.5% purity) in 400 mL of aqua regia under stirring. After 24 h, the obtained solution was filtered and 0.2 g of metallic iron (Fe)

was added to the solution. After homogenization, ultra-pure water was added to a volume of 2 L. Thus, a solution with 2.7 g/L of vanadium and 0.1 g/L of iron was obtained. Subsequently, based on another study already carried out [32], the pH and the redox potential (φ) were corrected to obtain V(IV) and Fe(II) by the addition of a sodium hydroxide (NaOH) solution (10 mol/L) and sodium dithionite ($\text{Na}_2\text{S}_2\text{O}_4$) (1 mol/L), respectively.

The purification of a solution of the same composition using the same resins tested in the present work was investigated by VINCO et al [32]. In such work, the authors studied the influence of pH, ratio of resin mass to solution volume and system temperature, evaluating the sorption process through adsorption isotherms and the thermodynamic parameters involved.

2.2 Ionic exchange experiments and kinetic study

The kinetic experiments for iron and vanadium adsorption were performed from 30 to 1440 min. Tests were carried out in Erlenmeyer flasks (250 mL) submitted to the orbital shaker with a stirring speed of 200 r/min. A ratio of 1 g of resin to 50 mL of solution at pH 2.0 was used.

The separation coefficient of V ($\beta_{\text{V/Fe}}$) for each evaluated adsorption time was calculated by Eq. (1) [33,34]:

$$\beta_{\text{V/Fe}} = \frac{C_{\text{V,r}} C_{\text{Fe,s}}}{C_{\text{Fe,r}} C_{\text{V,s}}} \quad (1)$$

where $C_{\text{V,r}}$ and $C_{\text{Fe,r}}$ are the concentrations of V and Fe in the resin, respectively, and $C_{\text{V,s}}$ and $C_{\text{Fe,s}}$ are the concentrations of V and Fe in the solution, respectively.

Kinetic modeling was performed according to data obtained to investigate the adsorption mechanism, the rates control of mass transport and the chemical reaction process [31]. In the present study, four distinct kinetic models: pseudo-first order, pseudo-second order, Elovich and intraparticle diffusion, were used.

The kinetic models of pseudo-first and pseudo-second order are the most employed in the kinetic metal adsorption study [31,35]. They are widely used in the description of the adsorption rate in liquid–solid type interactions, both being obtained from the integration of Eq. (2) [36]:

$$\frac{dq_t}{dt} = k_n (q_e - q_t)^n \quad (2)$$

where q_e and q_t are the amount of solute adsorbed per mass of adsorbent (mg/g) at equilibrium and time t (min), respectively, and k_n is the constant rate of the pseudo- n th order kinetic model (min^{-1}).

LAGERGREN [37] showed the obtained equation from the integration of Eq. (2) at $n=1$ under boundary conditions of: $t=0$, $q_t=0$ and $t=t$, $q_e=q_t$, naming the model of pseudo-first order (Eq. (3)) [36]. It is assumed that the adsorption processes that best fit this model have the adsorption driven by the mass concentration gradient [38]. Therefore, this model is more appropriate for the most initial steps in the adsorption process [39], since in more advanced stages the change in the concentration of metal ions in solution, in accordance with the fall in the number of active sites available in the resin, makes the model less applicable [40].

$$\ln(q_e - q_t) = \ln q_e - k_1 t \quad (3)$$

where k_1 is the equilibrium rate constant of the pseudo-first order equation (min^{-1}).

A linear model (Eq. (3)) might be rearranged to a non-linear form (Eq. (4)):

$$q_t = q_e [1 - \exp(-k_1 t)] \quad (4)$$

HO and MCKAY [41] integrated Eq. (2) assuming $n=2$ and using the same boundary conditions of LAGERGREN [37], thus obtaining an expression for the pseudo-second order model (Eq. (5)). According to this model, the rate of pseudo-second order reactions is predominantly related to the amount of metal ions that are on the surface of the adsorbent [38]. This model assumes that there is the occurrence of two reactions, being balance quickly reached by the first, and a second slower, which can extend for a long period of time, as chemisorption works as the determining step [40,42].

$$q_t = \frac{k_2 q_e^2 t}{k_2 q_e t + 1} \quad (5)$$

where k_2 is the equilibrium rate constant of the pseudo-second order equation ($\text{g}/(\text{mg} \cdot \text{min})$).

The nonlinear expression of the pseudo-second order model (Eq. (5)) can then be rearranged to obtain a linearized model (Eq. (6)):

$$\frac{t}{q_t} = \frac{1}{k_2 q_e^2} + \frac{1}{q_e} t \quad (6)$$

In these two models, however, through all

stages of the adsorption process, such as diffusion in the film, adsorption and intraparticle diffusion, the adsorption mechanism cannot be identified [35,43].

The kinetics rate of chemisorption of Elovich (Eq. (7)) distinguishes from previous models to deal with an exponential drop in the adsorption rate over time [44].

$$\frac{dq_t}{dt} = \alpha \exp(-\beta q_t) \quad (7)$$

where α is the constant of initial sorption rate ($\text{mg}/(\text{g}\cdot\text{min})$) and β is the constant of desorption (g/mg), which is related to the extension of surface coverage and activation energy for chemisorption.

CHIEN and CLAYTON [45] integrated Eq. (7) using the following boundary conditions: $t=0, q_t=0$ and $t=t, q_t=q_t$. They assumed $\alpha\beta t \gg 1$, obtaining the linearized expression for the Elovich model (Eq. (8)):

$$q_t = \frac{1}{\beta} \ln(\alpha\beta) + \frac{1}{\beta} \ln t \quad (8)$$

Regarding the mechanism related to the adsorption process of metals in adsorbents, four primordial stages are involved: (1) diffusion of metal ions to the liquid film on the surface of the adsorbent solid material; (2) diffusion of these metal ions through the superficial liquid film; (3) adsorption of the ions at the active sites of the adsorbent surface, a process of physical or chemical nature; (4) diffusion of ions through the pores of the adsorbent particles [46]. The diffusion rate of intraparticle mass (Eq. (9)) proposed by WEBER and MORRIS [47] predicts that the intraparticle diffusion stage is the limiting step of the adsorption process when the kinetic data are suitable for their model, i.e., when the amount of metal ions adsorbed by adsorbent as function of the square root of the contact time results in a straight line.

$$q_t = k_p t^{1/2} + C \quad (9)$$

where k_p is the constant of the intraparticle diffusion rate ($\text{mg}/(\text{g}\cdot\text{min}^{1/2})$), and C is a constant that reflects the effect of the limit layer, and the greater its value is, the greater the contribution of surface adsorption in the rate limitation is [46].

2.3 Chemical analysis

Samples before and after experiments were

analyzed by atomic absorption spectrometry equipment (AAS) (SHIMADZU AA-7000). The characterization of the resins before and after experiments was carried out in scanning electron microscopy (SEM) analyzer coupled to an energy dispersive spectroscopy (EDS) (Phenom ProX equipment) and infrared spectroscopy by Fourier transform (FT-IR) (Bruker Tensor 27 spectrometer). For FT-IR analysis, the resins were ground to make KBr tablets.

3 Results and discussion

3.1 Adsorption

The effect of time on vanadium and iron adsorption was studied at pH 2.0, 1 g of resin and 50 mL of solution at 298 K. The use of pH 2.0 is in agreement with the study carried out previously, which demonstrated the influence of pH on the recovery of these metals [32]. In this work, it was demonstrated within the range of pH evaluated (0.5–2.0) that pH 2.0 favored the adsorption of vanadium ions by the resins, providing the highest percentage of recovery. The recoveries of metals adsorbed by the resins as a function of time are depicted in Table 1. In 60 min, the TP 209 XL resin recovered 6.7% of vanadium in the solution. After 90 min, it increased to 25.8%, reaching a maximum in 180 min (31.4%). The resin TP 207 reached 22.5% of vanadium extraction in 30 min of contact and only in 420 min it reached a maximum recovery value (31.8%). After these maximums, both maintained a behavior close to stability.

The resins TP 209 XL and TP 207 showed a similar vanadium recovery in 1440 min (30.4 and 30.5%, respectively). Iron extraction, however, was 41.5% by TP 209XL, up to 9% higher than that of TP 207 (32.5%). This was reflected in low vanadium-to-iron separation coefficients, especially after 420 min of contact between the resin and the solution (Table 1). It is also noted that, for the case of TP 207 resin, the best separation between the two metals occurred in the first 30 min, where the $\beta_{V/Fe}$ was equal to 9.1, the highest value obtained among all those calculated.

Although with the same functional group and the same matrix composition, it is possible to notice a difference in the amount of vanadium and iron ions adsorbed by TP 209 XL and TP 207 chelating resins. ZAINOL and NICOL [48] also observed

similar behavior, who compared five resins functionalized by iminodiacetic acid (Amberlite IRC 748, Lewatit TP 207, Lewatit TP 208, Purolite S 930 and Lewatit TP 207 Monoplus) in the recovery of nickel and cobalt. The authors demonstrated that, despite having the same functional group, the performance of each one was different. Probably it occurs due to oscillation in the synthesis that could result in variations in the matrix crosslinking, density of functional groups and even the size of each particle.

In the case of M4195 and S 200 H resins, in contrast, the recovery of vanadium ions adsorbed achieved the equilibrium after 60 min of contact. These two resins were more selective for vanadium than iron in comparison to TP 207 and TP 209 XL, as depicted in Table 1, where there are higher values of $\beta_{V/Fe}$ related to the TP 209 XL and TP 207 resins. The recovery of vanadium by the M4195 resin reached equilibrium with adsorption efficiency up to about 45%, while the iron adsorption reached about 14%. The adsorption efficiencies of vanadium and iron by S 200 H were 35.5% and 7.2% at contact time of 60 min, respectively.

The pH of the solution was monitored over time, which is presented in Fig. 2. For all resins studied, it can be seen that there is an initial drop in the pH value, followed by a plateau. This behavior is explained by the fact of the H^+ ions initially occupied the functional groups of the resins and then are released into the solution due to the

exchange with vanadium and iron ions. This makes the solution more acidic. Even, the stabilization of the pH after the fall over time is in accordance with the stabilization of metals adsorption.

According to data presented in Fig. 2 and Table 1, although their behaviors are associated, the extraction percentage of metals by each resin is not proportional to decrease degree of pH of the medium, that is, how much H^+ is released into the solution. It can be visualized by the data from the M4195 resin, which demonstrates that, even though the resin that presented the greatest extraction of vanadium from the solution, it was the one that resulted in the lowest pH drop among the four resins analyzed.

The differences between the pH values among the resins are probably due to their exchange mechanism. For chelating resins (TP 209 XL, TP 207 and M4195), the decrease in pH was less pronounced in relation to the cation exchange resin S 200 H in which, after 30 min, a pH drop from 2.0 to 0.6 was observed (Fig. 2). This phenomenon can be explained by the adsorption of the metallic ions exclusively by ion exchange with the H^+ ions. That is, since it is not a chelating resin, the only way to recover metals in solution is through the ion exchange process, with a greater release of H^+ ions. Among the chelating resins, TP 207 and TP 209 XL had similar pH values over time (pH 1.2) due to the same functional group. For M4195 chelating resin, the pH reached 1.4 as the reaction achieved the equilibrium.

Table 1 Recoveries of V and Fe ions adsorbed by resins and separation coefficient ($\beta_{V/Fe}$) as function of contact time

Time/ min	TP 209 XL			TP 207			M4195			S 200 H		
	$\eta_V/\%$	$\eta_{Fe}/\%$	$\beta_{V/Fe}$									
30	3.8	5.2	0.7	22.5	3.1	9.1	35.4	10.3	4.8	34.7	6.8	7.3
60	6.7	10.3	0.6	24.1	5.8	5.2	40.2	15.2	3.8	35.5	7.2	7.1
90	25.8	11.3	2.7	25.6	7.9	4.0	42.5	14.5	4.4	38.0	9.0	6.2
120	30.9	16.2	2.3	28.9	9.9	3.7	42.1	13.8	4.6	36.9	10.8	4.8
180	31.4	24.4	1.4	28.4	12.8	2.7	43.2	13.6	4.8	35.8	11.5	4.3
300	28.5	35.4	0.7	30.4	17.2	2.1	43.3	14.7	4.4	35.9	10.5	4.8
420	30.1	38.3	0.7	31.8	29.3	1.1	45.9	14.5	5.0	35.0	10.5	4.6
540	29.9	39.7	0.6	31.7	31.4	1.0	45.0	14.7	4.7	33.4	11.5	3.9
960	28.3	40.9	0.6	31.1	30.9	1.0	45.5	13.7	5.3	33.7	11.4	3.9
1440	30.4	41.5	0.6	30.5	32.5	0.9	41.7	14.2	4.3	36.9	10.3	5.1

η_V is recovery of V, and η_{Fe} is recovery of Fe

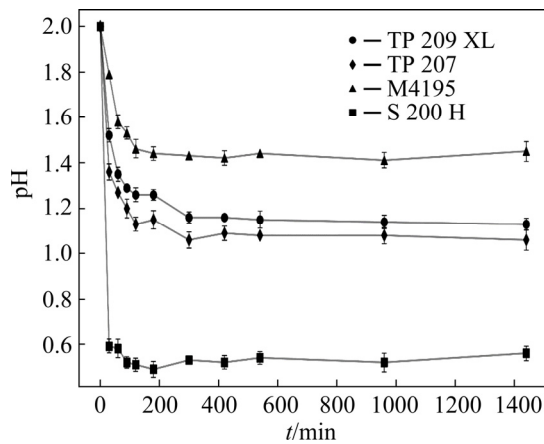


Fig. 2 Variation of pH of medium as function of contact time for resins under experimental conditions of 298 K, 1 g of resin in 50 mL of solution, and initial pH of 2.0

3.2 Kinetic modeling

Kinetic parameters were obtained through the plots of the linearized models of pseudo-first order (Eq. (3): $\ln(q_e - q_t)$ vs t), pseudo-second order (Eq. (6): t/q_t vs t), Elovich (Eq. (8): q_t vs $\ln t$) and intraparticle diffusion (Eq. (9): q_t vs $t^{1/2}$). The data plotted for each kinetic model is presented in Fig. 3 (q_t vs t). Table 2 shows the parameters for each kinetic model for all resins studied. The choice of which kinetic model best explains the adsorption behavior of vanadium and iron ions by resins must be based on not only the value of the determination coefficient obtained with the linearization of the models, but also how the models will be adjusted over time to all experimental points, and whether the calculated kinetic parameters are consistent.

Parameters depicted in Table 2 show that the adsorption of vanadium by the four resins follows a pseudo-second order kinetics, in view of the higher

values of the correlation coefficient (R^2) obtained by the linearization of this model. A best fit in this model indicates that the adsorption of vanadium ions in the functional groups of the resins has their rate controlled by the amount of the metallic ions that are on the surface of the resin and, also, by the valence forces that occur due to the sharing of electrons between the metal ions and the functional groups [49].

It is indicated that in the first hours of contact of the solution with the resin there is a fast adsorption of vanadium ions. However, as the active sites are occupied by the metal, large amount of ions result in a slower adsorption rate. This is also assumed by the model, which reiterates that the balance of the process is quickly achieved by a first ion exchange reaction that occurs in the system. Given the high correlation of the data to the model (all close to 1), the values for the calculated amount of ions adsorbed in the equilibrium q_e are in agreement with those verified experimentally. Figures 3(a, c, e, g) demonstrated that the pseudo-second order model exhibited a stability behavior when the adsorption of vanadium ions had reached equilibrium after 240 min for all resins.

The adsorption kinetics of iron is also explained by the pseudo-second order model for the four resins. For the TP 207 resin, although the correlation coefficients obtained for the pseudo-first and pseudo-second order kinetics are equal (0.992), the analysis in Fig. 3(d) shows that the best fit of the pseudo-second order model to the experimental points when compared to the pseudo-first order. In addition, the system still seems not to reach equilibrium at 1440 min, since the adsorption rate is increasing. Therefore, although the q_e value

Table 2 Kinetic parameters calculated from pseudo-first order, pseudo-second order, Elovich and intraparticle diffusion models for vanadium and iron elements for each of studied resins

Resin	Metal	Pseudo-first order			Pseudo-second order			Elovich			Intraparticle diffusion		
		k_1/min^{-1}	$q_e/(\text{mg}\cdot\text{g}^{-1})$	R^2	$k_2/(\text{g}\cdot\text{mg}^{-1}\cdot\text{min}^{-1})$	$q_e/(\text{mg}\cdot\text{g}^{-1})$	R^2	$\alpha/(\text{mg}\cdot\text{g}^{-1}\cdot\text{min}^{-1})$	$\beta/(\text{g}\cdot\text{mg}^{-1})$	R^2	$k_p/(\text{g}\cdot\text{mg}^{-1}\cdot\text{min}^{-1/2})$	C	R^2
TP 209 XL	V	3.13×10^{-2}	162.26	0.919	9.10×10^{-4}	54.35	0.997	1.76×10^0	0.040	0.965	6.44	-15.67	0.990
	Fe	4.47×10^{-3}	0.95	0.983	9.29×10^{-3}	0.91	0.998	9.41×10^{-3}	3.82	0.951	0.050	-0.21	0.977
TP 207	V	6.86×10^{-3}	20.07	0.982	7.99×10^{-4}	58.95	0.999	1.26×10^2	0.16	0.981	1.11	35.05	0.978
	Fe	2.33×10^{-3}	0.60	0.992	3.24×10^{-3}	0.82	0.992	5.44×10^{-3}	6.05	0.966	0.019	-0.0085	0.941
M4195	V	7.89×10^{-3}	20.95	0.916	1.24×10^{-3}	84.42	0.999	2.36×10^8	0.29	0.840	1.70	58.19	0.872
	Fe	2.29×10^{-3}	0.039	0.747	4.85×10^{-1}	0.27	0.999	9.02×10^3	73.37	0.768	0.0017	0.23	0.759
S 200 H	V	1.11×10^{-2}	9.19	0.888	3.21×10^{-3}	67.57	0.999	2.68×10^4	0.19	0.823	1.29	55.35	0.781
	Fe	1.58×10^{-2}	0.19	0.954	2.12×10^{-1}	0.21	0.993	7.63×10^{-3}	13.54	0.950	0.012	0.050	0.928

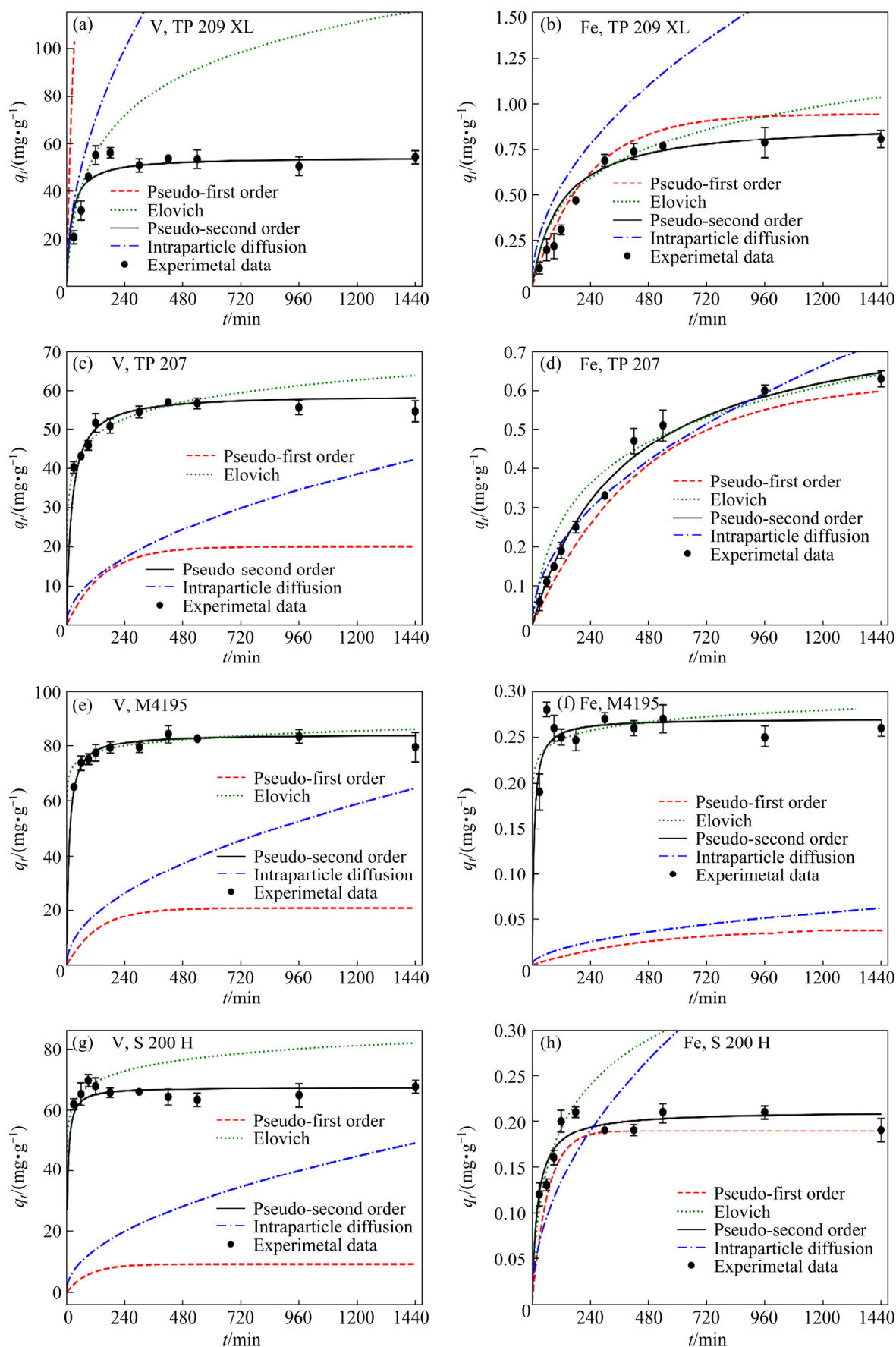


Fig. 3 Kinetic models obtained for TP 209 XL, TP 207, M4195 and S 200 H resins

calculated by the pseudo-first order model (0.60 mg/g) is apparently closest to the presented data, it does not represent the actual amount of iron ions adsorbed in the equilibrium, which is probably better explained by the value obtained by the pseudo-second order model (0.82 mg/g). FATIMA et al [50] investigated the adsorption kinetics of some metals when using a cationic exchange resin functionalized by the sulfonic acid group. It was shown that, for Fe(II) recovery, the pseudo-second order model is also the one that best relates to the data obtained, indicating that chemical sorption may be the limiting step of the reaction rate.

3.3 Characterization of resins in adsorption

In order to understand the chemical bond connection that occurs between the metal ions and the resins, FT-IR (Fig. 4) and SEM-EDS (Fig. 5) measurements were performed before and after the adsorption.

FT-IR spectra show strong and wide bands at 3431 cm^{-1} . These are related both to the vibrations of the hydroxyl groups (O—H) and the stretching

vibrations of N—H bonds [51,52]. The peaks at 3023 cm^{-1} come from the asymmetric stretching of the $\nu_{\text{as}}(\text{C—H})$ from the C—H bonds present in the aromatic rings [52]. The hydrogen vibration band outside the plane of the aromatic ring $\delta(\text{C—H})$ is responsible for the appearance of the observed peaks at 700 cm^{-1} (Figs. 4(a) and (b)) and 704 cm^{-1} (Fig. 4(c)) [53]. The peaks at 2926 cm^{-1} refer to $\nu_{\text{as}}(-\text{CH}_2)$, an antisymmetric stretching vibration of the $-\text{CH}_2$ groups [52,54]. Meanwhile, M4195 resin (Fig. 4(c)) also presents a peak at 1452 cm^{-1} , which is related to the asymmetric scissoring vibration band of $\delta_{\text{as}}(-\text{CH}_2)$ groups [51,55].

Peaks at 1630 and 1732 cm^{-1} (Figs. 4(a) and (b)) indicate the presence of hydrophilic groups (C=O) at $1620\text{--}1640\text{ cm}^{-1}$ and $1710\text{--}1740\text{ cm}^{-1}$, being the second one characterizing the presence of C=O of $-\text{COOH}$ groups [56,57]. Besides, peaks at 1385 cm^{-1} are associated to the symmetric deformation of carboxylate ions ($\nu_{\text{s}}(-\text{COO}^-)$) [58]. The presence of C=O band in the TP 209 XL and TP 207 resins is also confirmed by peaks at 1225 cm^{-1} [59].

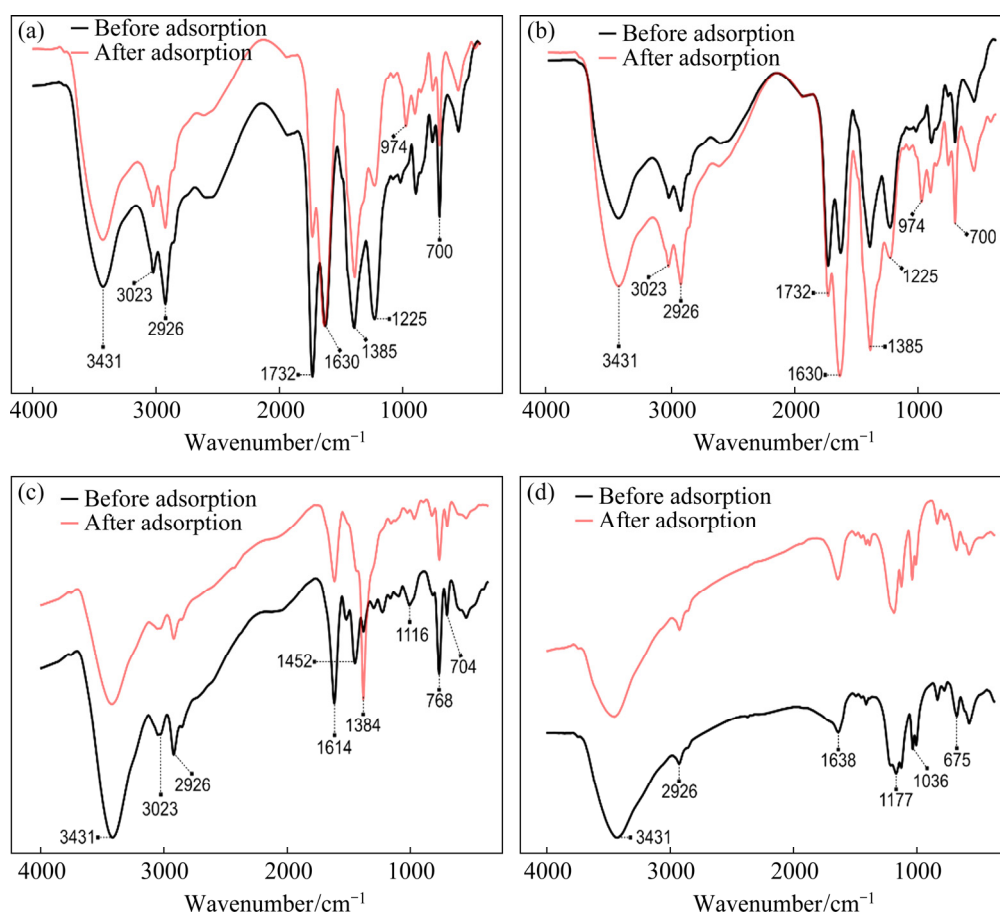


Fig. 4 FT-IR spectra before and after adsorption experiments for TP 209 XL (a), TP 207 (b), M4195 (c) and S 200 H (d) resins

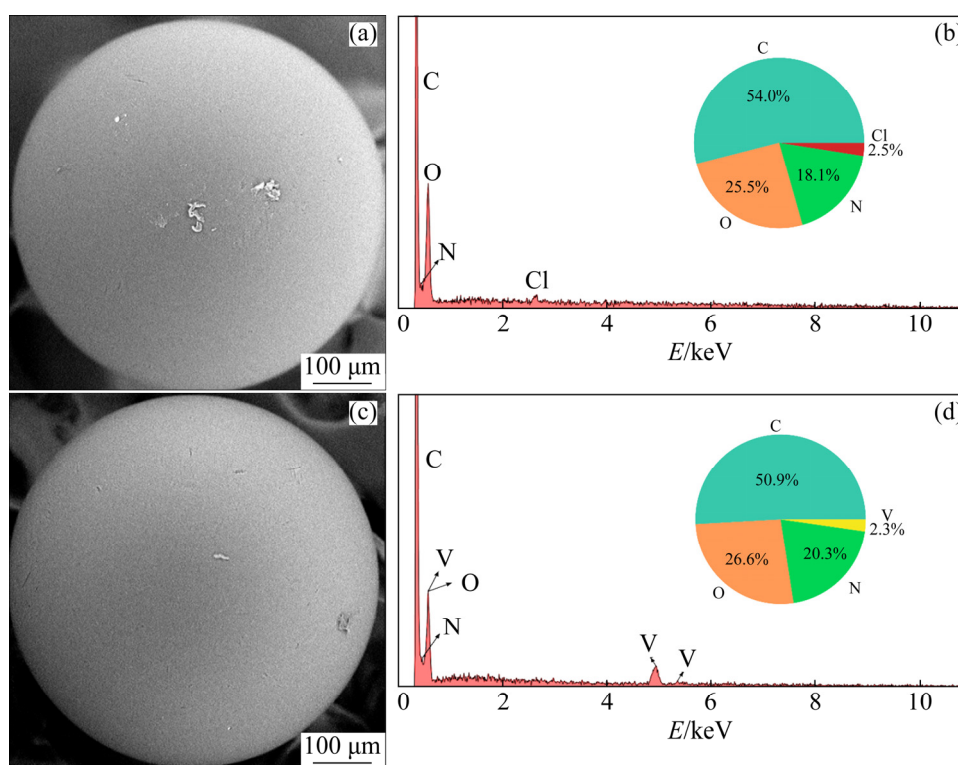


Fig. 5 SEM images (a, c) and their respective EDS spectra (b, d) for TP 209 XL resin before (a, b) and after (c, d) adsorption experiments

In Fig. 4(d), the presence of the $-\text{SO}_3\text{H}$ in S 200 H resin can be identified by the specific peaks of this group at 1177 , 1036 and 675 cm^{-1} [60]. The peak at 1117 cm^{-1} refers to the asymmetric stretching mode of the $\text{S}=\text{O}$ bond, while the 1036 cm^{-1} occurs due to the symmetric stretching mode in the same bond [61]. The peak at 1639 cm^{-1} must be associated to the $\text{C}=\text{C}$ bond [62].

Pyridine groups of M4195 resin (Fig. 4(c)) were identified through the vibration at 1614 cm^{-1} , reflecting the $\text{C}=\text{N}$ bond [55]. The peaks at 1116 and 768 cm^{-1} are related, respectively, to $\text{C}-\text{N}$ and $\text{C}-\text{H}$ bonds of the pyridine molecule [55]. The peak at 1384 cm^{-1} is also a $\text{C}-\text{N}$ correspondent stretching mode [63]. It becomes strong and quite accentuated in the spectrum corresponding to the M4195 resin after the adsorption experiments, probably due to the adsorption and complexation of vanadium ions by the functional group.

The presence of peaks at 974 cm^{-1} shown in TP 209 XL and TP 207 resins (Figs. 4(a) and (b), respectively) after the adsorption process can be attributed to the deformation vibrations of the copolymer benzene ring (ST-DVB), which forms the matrix of both resins [52]. The spectra after

contact with the solution (Figs. 4(a–c)) were altered in several peaks, either by attenuation or by intensification. It corroborates the fact that, in the functional group of chelating resins, complexation with metals also occurs and is not just an adsorption process.

TP 207 resin was studied for copper recovery with iron as an impurity in the work of BOTELHO JUNIOR et al [64]. The authors obtained FT-IR spectra with peaks at values very close to those shown in Fig. 4(b) and also demonstrated that, when in contact with the copper and iron ions, the resin undergoes a process of coordination between the functional group and the solution ions.

SOFIŃSKA-CHMIEL and KOŁODYŃSKA [65] evaluated the spectra of the M4195 resin before and after the adsorption of metals such as copper and zinc and the behavior was analogous to that shown in Fig. 4(c). The change in peak intensity in the region between 1250 and 1650 cm^{-1} was attributed to the formation of bands and coordination links of these functional groups with the adsorbed metals.

WOŁOWICZ and HUBICKI [66] studied the chelating resin TP 220 with bis-picolylamine functional group and compared its FT-IR spectrum

with that of M4195. The authors also suggested that the peak attenuation in the region regarding the vibration of the atoms of the functional groups was due to their participation in the bond with the recovered metal (Pd).

These results corroborate with those presented in Section 3.1, where it was shown that the recovery of metal ions by chelating resins occurred not only by ion exchange, but also by complexing these with the functional group.

In the present study, the resins before and after the experiments were analyzed by SEM–EDS to investigate the adsorption process. None of the resins showed physical changes on their surfaces after the experiments. Although reported as macroporous resins [67], a very smooth surface was found, most of them in a diameter range of 300–400 μm . As the SEM image and EDS spectra were similar among the resins studied, Fig. 5 shows only the data obtained for TP 209 XL resin (the others are shown in the Supplementary materials).

TP 209 XL and TP 207 resins have quite similar EDS spectra. Major elements are, respectively, carbon (54.0%, 45.7%), oxygen (25.5%, 30.2%) and nitrogen (18.1%, 18.0%), as expected, once these consist of their functional groups (iminodiacetic acid in Fig. 1). Carbon (50.5%), nitrogen (22.1%) and oxygen (23.7%) are also the major elements in the M4195 resin. Finally, major elements of the S 200 H resin are carbon (48.8%), oxygen (33.7%) and sulfur (17.5%), which are coherent with the sulfonic acid functional group. Chlorine is also present in the spectra of TP 209XL, TP 207 and M4195 resins, and probably related to the washing process with HCl solution.

Atomic proportions have non-significant changes after experiments. Peaks of vanadium were observed after adsorption experiments. The cationic resin S 200 H showed the presence of Na element, used to adjust the pH (NaOH).

Although iron was adsorbed, it was not identified in any of the resins studied by means of semi-quantitative EDS after the adsorption experiments due to the sensitivity of the technique. An important observation is that the quantification given by the EDS must be considered as a qualitative guidance of the proportions of those elements, as this technique is not sufficiently accurate to serve as a chemical quantification.

4 Conclusions

(1) The adsorption of iron and vanadium was studied using four ion exchange resins. The investigation of the process over time revealed that the resins TP 209 XL and TP 207 demonstrated different kinetic behaviors and that the resins M4195 and S 200 H tend to equilibrate from the first 30 min of contact with the solution. M4195 resin, in particular, had the highest vanadium recovery (about 45% of all vanadium) and the lowest iron adsorption (about 14%).

(2) Monitoring the behavior of pH over time showed that chelating resins, due to coordination interaction with metals, release less H^+ ions into the medium as the ions are adsorbed on their functional groups in relation to the cationic exchange resin.

(3) Regarding the reaction kinetics, it was shown that the adsorption of both metals is better explained by the mechanism proposed by the pseudo-second order model, indicating that the adsorption rate of these metals by the four resins evaluated is controlled by a process of chemisorption.

(4) The change in intensity and displacement of some peaks in the spectra generated by the FT-IR analysis for the resins, before and after the tests, corroborated the understanding that complexation occurs in chelating resins.

(5) This study provides fundamental information for scaling this technique to industrial processes. This is because knowledge of kinetic parameters is essential in equipment sizing and performance calculations, which form the basis for determining the investment's potential.

Acknowledgments

J. H. VINCO is grateful for the grant provided by Conselho Nacional de Desenvolvimento Científico e Tecnológico (CNPq, grant 130978/2020-5), to the Fundação de Amparo à Pesquisa do Estado de São Paulo (FAPESP, grant 2019/11866-5), and to CAPES for the financial support. We would also like to thank Mr. Sai-qian YUAN and the anonymous reviewers, where comments have contributed to the improvement of this paper.

Supplementary materials

Supplementary materials in this work can

be found at: <http://www.yxabcn.com/download/27-p2438-2021-0739-supplemental materials.pdf>.

References

- [1] MOSKALYK R R, ALFANTAZI A M. Processing of vanadium: A review [J]. *Minerals Engineering*, 2003, 16(9): 793–805.
- [2] SWINBOURNE D R, RICHARDSON T, CABALTEJA F. Understanding ferrovanadium smelting through computational thermodynamics modelling [J]. *Mineral Processing of Extractive Metallurgy*, 2016, 125(1): 45–55.
- [3] GILLIGAN R, NIKOLOSKI A N. The extraction of vanadium from titanomagnetites and other sources [J]. *Minerals Engineering*, 2020, 146: 106106.
- [4] ALGAR V. Investing in the energy storage future — Resources rising stars 2017 [M]. Perth: Australian Vanadium Limited, 2017.
- [5] Bushveld Minerals. Corporate presentation 2021. [EB/OL]. 2021–02–19. <http://www.bushveldminerals.com/wp-content/uploads/2021/03/Bushveld-Minerals-February-Corporate-Presentation.pdf>.
- [6] CHOI C, KIM S, KIM R, CHOI Y, KIM S, JUNG H Y, YANG J H, KIM H T. A review of vanadium electrolytes for vanadium redox flow batteries [J]. *Renewable and Sustainable Energy Reviews*, 2017, 69: 263–274.
- [7] MAHANDRA H, SINGH R, GUPTA B. Recovery of vanadium(V) from synthetic and real leach solutions of spent catalyst by solvent extraction using Cyphos IL 104 [J]. *Hydrometallurgy*, 2020, 196: 105405.
- [8] WANG M Y, ZHANG G Q, WANG X W, ZHANG J L. Solvent extraction of vanadium from sulfuric acid solution [J]. *Rare Metals*, 2009, 28(3): 209–211.
- [9] TAVAKOLIKHALEDI M. Vanadium: Leaching and solvent extraction [D]. Vancouver: University of British Columbia, 2014.
- [10] LI X B, WEI C, DENG Z G, LI C X, FAN G, LI M T, HUANG H. Recovery of vanadium from H₂SO₄–HF acidic leaching solution of black shale by solvent extraction and precipitation [J]. *Metals*, 2016, 6(3): 63.
- [11] DENG Z G, WEI C, FAN G, LI M T, LI C X, LI X B. Extracting vanadium from stone-coal by oxygen pressure acid leaching and solvent extraction [J]. *Transactions of Nonferrous Metals Society of China*, 2010, 20: s118–s122.
- [12] LI X B, WEI C, WU J, LI C X, LI M T, DENG Z G, XU H S. Thermodynamics and mechanism of vanadium (IV) extraction from sulphate medium with D2EHPA, EHEHPA and CYANEX 272 in kerosene [J]. *Transactions of Nonferrous Metals Society of China*, 2012, 22(2): 461–466.
- [13] NAVARRO R, GUZMAN J, SAUCEDO I, REVILLA J, GUIBAL E. Vanadium recovery from oil fly ash by leaching, precipitation and solvent extraction processes [J]. *Waste Management*, 2007, 27(3): 425–438.
- [14] HU B, CHEN B F, ZHANG C D, DAI Y Y, WANG M Y, WANG X W. Separation and recovery of chromium from solution after vanadium precipitation [J]. *Mining, Metallurgy & Exploration*, 2021, 38(1): 289–297.
- [15] PENG H, YANG L, WANG L, GUO J, LI B. Recovery of vanadium with urea in acidic medium [J]. *Environmental Chemistry Letters*, 2019, 17(4): 1867–1871.
- [16] DRUŻYŃSKI S, MAZUREK K, BIAŁOWICZ K. The use of ion exchange in the recovery of vanadium from the mass of a spent catalyst used in the oxidation of SO₂ to SO₃ [J]. *Polish Journal of Chemical Technology*, 2014, 16(2): 69–73.
- [17] LI Q G, ZENG L, XIAO L S, YANG Y N, ZHANG Q X. Completely removing vanadium from ammonium molybdate solution using chelating ion exchange resins [J]. *Hydrometallurgy*, 2009, 98(3/4): 287–290.
- [18] ZHU X B, LI W, TANG S, ZENG M J, BAI P Y, CHEN L J. Selective recovery of vanadium and scandium by ion exchange with D201 and solvent extraction using P507 from hydrochloric acid leaching solution of red mud [J]. *Chemosphere*, 2017, 175: 365–372.
- [19] LI M, ZHANG B G, ZOU S Q, LIU Q S, YANG M. Highly selective adsorption of vanadium (V) by nano-hydrous zirconium oxide-modified anion exchange resin [J]. *Journal of Hazardous Materials*, 2020, 384: 121386.
- [20] ZHU X Z, HUO G S, NI J, SONG Q. Removal of tungsten and vanadium from molybdate solutions using ion exchange resin [J]. *Transactions of Nonferrous Metals Society of China*, 2017, 27(12): 2727–2732.
- [21] ZHANG J H, ZHANG W, ZHANG L, GU S Q. A critical review of technology for selective recovery of vanadium from leaching solution in V₂O₅ production [J]. *Solvent Extraction and Ion Exchange*, 2014, 32(3): 221–248.
- [22] SHOLL D S, LIVELY R P. Seven chemical separations to change the world [J]. *Nature*, 2016, 532(7600): 435–437.
- [23] CYGANOWSKI P, DZIMITROWICZ A. A mini-review on anion exchange and chelating polymers for applications in hydrometallurgy, environmental protection, and biomedicine [J]. *Polymers*, 2020, 12(4): 784.
- [24] ALEXANDRATOS S D. Ion-exchange resins: A retrospective from industrial and engineering chemistry [J]. *Industrial & Engineering Chemistry Research*, 2009, 48: 388–398.
- [25] NASEF M M, UJANG Z. Ion exchange technology I—Theory and materials [M]. Heidelberg: Springer, 2013: 1–39.
- [26] KAGAYA S, GEMMEI-IDE M, INOUE Y. Encyclopedia of polymeric nanomaterials [M]. Heidelberg: Springer, 2015: 369–378.
- [27] SIROLA K, LAATIKAINEN M, LAHTINEN M, PAATERO E. Removal of copper and nickel from concentrated ZnSO₄ solutions with silica-supported chelating adsorbents [J]. *Separation and Purification Technology*, 2008, 64(1): 88–100.
- [28] ULLOA L, MARTÍNEZ-MINCHERO M, BRINGAS E, COBO A, SAN-ROMÁN M F. Split regeneration of chelating resins for the selective recovery of nickel and copper [J]. *Separation and Purification Technology*, 2020, 253: 117516.
- [29] BATOOL F, AKBAR J, IQBAL S, NOREEN S, BUKHARI S N A. Study of isothermal, kinetic, and thermodynamic parameters for adsorption of cadmium: An overview of linear and nonlinear approach and error analysis [J]. *Bioinorganic Chemistry and Applications*, 2018, 2018: 3463724.
- [30] GAUTAM R K, CHATTOPADHYAYA M C. Nanomaterials for wastewater remediation [M]. Amsterdam: Elsevier, 2016:

- 79–109.
- [31] FEBRIANTO J, KOSASIH A N, SUNARSO J, JU Y H, INDRASWATI N, ISMADJI S. Equilibrium and kinetic studies in adsorption of heavy metals using biosorbent: A summary of recent studies [J]. *Journal of Hazardous Materials*, 2009, 162(2/3): 616–645.
- [32] VINCO J H, BOTELHO JUNIOR A B Jr, DUARTE H A, ESPINOSA, D C R, TENÓRIO, J A S. Purification of an iron contaminated vanadium solution through ion exchange resins [J]. *Minerals Engineering*, 2022, 176: 107337.
- [33] ZHANG Y, ZHANG T A, DREISINGER D, ZHOU W H, XIE F, LV G Z, ZHANG W G. Chelating extraction of vanadium(V) from low pH sulfuric acid solution by Mextral 973H [J]. *Separation and Purification Technology*, 2018, 190: 123–135.
- [34] TOKUYAMA H, NII S, KAWAIZUMI F, TAKAHASHI K. Process development for recovery of vanadium and nickel from heavy oil fly ash by leaching and ion exchange [J]. *Separation Science and Technology*, 2003, 38: 1329–1344.
- [35] ANASTOPOULOS I, BHATNAGAR A, LIMA E C. Adsorption of rare earth metals: A review of recent literature [J]. *Journal of Molecular Liquids*, 2016, 221: 954–962.
- [36] MOUSSOUT H, AHLAFI H, AAZZA M, MAGHAT H. Critical of linear and nonlinear equations of pseudo-first order and pseudo-second order kinetic models [J]. *Karbala International Journal of Modern Science*, 2018, 4(2): 244–254.
- [37] LAGERGREN S. About the theory of so-called adsorption of soluble substances [J]. *Handlingar*, 1898, 24(4): 1–39.
- [38] ARROYO F, MORILLO J, USERO J, ROSADO D, EL-BAKOURI H. Lithium recovery from desalination brines using specific ion-exchange resins [J]. *Desalination*, 2019, 468: 114073.
- [39] SHEK T H, MA A, LEE V K C, MCKAY G. Kinetics of zinc ions removal from effluents using ion exchange resin [J]. *Chemical Engineering Journal*, 2009, 146(1): 63–70.
- [40] ABDELWAHAB O, AMIN N K, EL-ASHTOUKHY E S Z. Removal of zinc ions from aqueous solution using a cation exchange resin [J]. *Chemical Engineering Research and Design*, 2013, 91(1): 165–173.
- [41] HO Y S, MCKAY G. Pseudo-second order model for sorption processes [J]. *Process Biochemistry*, 1999, 34(5): 451–465.
- [42] KHAMBHATY Y, MODY K, BASHA S, JHA B. Kinetics, equilibrium and thermodynamic studies on biosorption of hexavalent chromium by dead fungal biomass of marine *Aspergillus niger* [J]. *Chemical Engineering Journal*, 2009, 145(3): 489–495.
- [43] CRINI G, BADOT P M. Application of chitosan, a natural aminopolysaccharide, for dye removal from aqueous solutions by adsorption processes using batch studies: A review of recent literature [J]. *Progress in Polymer Science (Oxford)*, 2008, 33(4): 399–447.
- [44] SIU P C C, KOONG L F, SALEEM J, BARFORD J, MCKAY G. Equilibrium and kinetics of copper ions removal from wastewater by ion exchange [J]. *Chinese Journal of Chemical Engineering*, 2016, 24(1): 94–100.
- [45] CHIEN S H, CLAYTON W R. Application of Elovich equation to the kinetics of phosphate release and sorption in soils [J]. *Soil Science Society of America Journal*, 1980, 44(2): 265–268.
- [46] PHOLOSI A, NAIDOO E B, OFOMAJA A E. Intraparticle diffusion of Cr(VI) through biomass and magnetite coated biomass: A comparative kinetic and diffusion study [J]. *South African Journal of Chemical Engineering*, 2020, 32: 39–55.
- [47] WEBER W J Jr, MORRIS J C. Kinetics of adsorption on carbon from solution [J]. *Journal of the Sanitary Engineering Division*, 1963, 89(2): 31–59.
- [48] ZAINOL Z, NICOL M J. Comparative study of chelating ion exchange resins for the recovery of nickel and cobalt from laterite leach tailings [J]. *Hydrometallurgy*, 2009, 96(4): 283–287.
- [49] PAN S Y, SYU W J, CHANG T K, LEE C H. A multiple model approach for evaluating the performance of time-lapse capsules in trapping heavy metals from water bodies [J]. *RSC Advances*, 2020, 10(28): 16490–16501.
- [50] FATIMA N, ZHANG Q, CHEN R R, YAN D X, ZHOU Q, LU X M, XIN J Y. Adsorption thermodynamics and kinetics of resin for metal impurities in bis(2-hydroxyethyl) terephthalate [J]. *Polymers*, 2020, 12(12): 1–12.
- [51] XIONG C H, LI Y L, WANG G T, FANG L, ZHOU S G, YAO C P, CHEN Q, ZHENG X M, QI D M, FU Y Q, ZHU Y E. Selective removal of Hg(II) with polyacrylonitrile-2-amino-1,3,4-thiadiazole chelating resin: Batch and column study [J]. *Chemical Engineering Journal*, 2015, 259: 257–265.
- [52] KOŁODYŃSKA D, HUBICKI Z, PASIECZNA-PATKOWSKA S. FT-IR/PAS studies of Cu(II)-EDTA complexes sorption on the chelating ion exchangers [J]. *Acta Physica Polonica A*, 2009, 116(3): 340–343.
- [53] GARCIA-VASQUEZ W, DAMMAK L, LARCHET C, NIKONENKO V, PISMENSKAYA N, GRANDE D. Evolution of anion-exchange membrane properties in a full scale electrodialysis stack [J]. *Journal of Membrane Science*, 2013, 446: 255–265.
- [54] KUĆ M, CIEŚLIK-BOCZULA K, ŚWIĄTEK P, JASZCZYŹYŃ A, GAŚSIOROWSKI K, MALINKA W. FTIR-ATR study of the influence of the pyrimidine analog of fluphenazine on the chain-melting phase transition of sphingomyelin membranes [J]. *Chemical Physics*, 2015, 458: 9–17.
- [55] KOŁODYŃSKA D, SOFIŃSKA-CHMIEL W, MENDYK E, HUBICKI Z. DOWEX M4195 and LEWATIT® MonoPlus TP 220 in Heavy Metal Ions Removal from Acidic Streams [J]. *Separation Science and Technology*, 2014, 49(13): 2003–2015.
- [56] WIERICIK P, FRĄCZEK B, CHROBOT P. Fouling of anion exchanger by image and FTIR analyses [J]. *Journal of Environmental Chemical Engineering*, 2020, 8(3): 103761.
- [57] TARCHITZKY J, LERNER O, SHANI U, ARYE G, LOWENGART-AYCICEGI A, BRENER A, CHEN Y. Water distribution pattern in treated wastewater irrigated soils: Hydrophobicity effect [J]. *European Journal of Soil Science*, 2007, 58(3): 573–588.
- [58] GRANADOS-OLIVEROS G, ORTEGA F M, PÁEZ-MOZO E, FERRONATO C, CHOVELON J M. Photoactivity of metal-phenylporphyrins adsorbed on TiO₂ under visible light

- radiation: Influence of central metal [J]. *The Open Materials Science Journal*, 2010, 4: 15–22.
- [59] XU Q W, LO J C C, LEE S W R. Directly printed hollow connectors for microfluidic interconnection with UV-assisted coaxial 3D printing [J]. *Applied Sciences*, 2020, 10(10): 1–13.
- [60] GHOSH S, DHOLE K, TRIPATHY M K, KUMAR R, SHARMA R S. FTIR spectroscopy in the characterization of the mixture of nuclear grade cation and anion exchange resins [J]. *Journal of Radioanalytical and Nuclear Chemistry*, 2015, 304(2): 917–923.
- [61] CAPRARESCU S, COROBEA M C, PURCAR V, SPATARU C I, IANCHIS R, VASILIEVICI G, VULUGA Z. San copolymer membranes with ion exchangers for Cu(II) removal from synthetic wastewater by electrodialysis [J]. *Journal of Environmental Sciences*, 2015, 35: 27–37.
- [62] MORSCH S, LIU Y W, LYON S B, GIBBON S R, GABRIELE B, MALANIN M, EICHHORN K J. Examining the early stages of thermal oxidative degradation in epoxy-amine resins [J]. *Polymer Degradation and Stability*, 2020, 176: 109147.
- [63] YANG L, MAY P W, YIN L, SMITH J A, ROSSER K N. Ultra fine carbon nitride nanocrystals synthesized by laser ablation in liquid solution [J]. *Journal of Nanoparticle Research*, 2007, 9(6): 1181–1185.
- [64] BOTELHO JUNIOR A B, VICENTE A A, ESPINOSA D C R, TENÓRIO J A S. Effect of iron oxidation state for copper recovery from nickel laterite leach solution using chelating resin [J]. *Separation Science and Technology*, 2020, 55(4): 788–798.
- [65] SOFIŃSKA-CHMIEL W, KOŁODYŃSKA D. Application of ion exchangers for the purification of galvanic wastewater from heavy metals [J]. *Separation Science and Technology*, 2018, 53(7): 1097–1106.
- [66] WOŁOWICZ A, HUBICKI Z. The use of the chelating resin of a new generation Lewatit MonoPlus TP-220 with the bis-picolylamine functional groups in the removal of selected metal ions from acidic solutions [J]. *Chemical Engineering Journal*, 2012, 197: 493–508.
- [67] Lewatit® MonoPlus TP 209 XL. Cologne, Germany. [EB/OL]. 2019–05–06. <https://lanxess.com/en/Products-and-Solutions/Products/LEWATIT-MonoPlus-TP-209-XL>.

离子交换树脂吸附酸性溶液中钒和铁的动力学模拟

José Helber VINCO, Amilton Barbosa BOTELHO JUNIOR, Heitor Augusto DUARTE,
Denise Croce Romano ESPINOSA, Jorge Alberto Soares TENÓRIO

Department of Chemical Engineering, Polytechnic School of the University of São Paulo (USP),
Rua do Lago, 250, 05508-080, São Paulo, SP, Brazil

摘要: 评价从含铁杂质的酸性溶液中选择性回收钒的吸附过程和反应动力学。研究 Lewatit® MonoPlus TP 209 XL、Lewatit® TP 207、Dowex™ M4195(螯合树脂)和 Lewatit® MonoPlus S 200 H (强阳离子交换树脂) 4 种工业树脂。在以下初始条件下进行批量实验: pH 值 2.0、温度 298 K、树脂与溶液的比例 1 g/50 mL。研究时间对吸附过程的影响, 分析 pH 值随时间的变化情况。随着吸附作用的发生, 与 S 200 H 树脂相比, 螯合树脂释放的 H⁺ 离子较少, 导致 pH 值降低较少。通过 FT-IR 和 SEM-EDS 对实验前后树脂的离子吸附行为进行评价。在所评价的动力学模型(准一级、准二级、Elovich 和颗粒内扩散模型)中, 准二级模型与 4 种树脂对钒和铁的吸附实验数据最吻合。M4195 树脂对钒的回收率最高, 对铁的吸附率最低。本文提供了对于工业应用至关重要的动力学数据。

关键词: 钒回收; 吸附; 螯合树脂; 金属离子; 阳离子交换树脂; 批量实验

(Edited by Wei-ping CHEN)